Lubricant transport across the piston ring with flat and triangular lubrication injection profiles on the liner in large two-stroke marine diesel engines

Overgaard, H.; Klit, P.; Vølund, A.

Published in:
Proceedings of the Institution of Mechanical Engineers, Part J: Journal of Engineering Tribology

Link to article, DOI:
10.1177/1350650117715151

Publication date:
2018

Document Version
Peer reviewed version

Journal Title
XX(X):1–10

DOI: 10.1177/ToBeAssigned
www.sagepub.com/
SAGE

Lubricant Transport across the Piston Ring with Flat and Triangular Lubrication Injection Profiles on the Liner in Large Two-Stroke Marine Diesel Engines.

H. Overgaard[1], P. Klit[1] and A. Vølund[2]

Abstract
A theoretical investigation of the lubricant transport across the top compression piston ring in a large two-stroke marine diesel engine is presented.

A numerical model for solving Reynolds equation between the piston ring and cylinder liner based on the finite difference method in 1D has been made. The model includes force equilibrium of the piston ring, perturbation of Reynolds equation and transient mass conservation. The model represents a new method of achieving mass conservation across the piston ring and between different time dependent positions.

For analyzing the lubricant transport across the piston ring two different kinds of initial lubricant profile on the liner and two different kinds of load are investigated i.e. a flat profile and an approximated triangular profile as well as no load and a combustion load based on a combustion pressure profile.

The impact from the different load conditions and different lubricant profiles on the liner are presented for film thicknesses, development in the lubricant profiles on the liner as well as the lubricant consumption at each stroke.

Keywords
lubricant transport, Reynolds equation, piston ring lubrication, finite difference method, lubricant injection, perturbation of Reynolds equation, hydrodynamic lubrication, flow continuity, lubricant starvation.

Introduction

Piston ring lubrication has previously been studied by numerous authors e.g. [1] where numerical schemes were developed to solve Reynolds equation simultaneously with the load equilibrium equation for one cycle.

A theoretical investigation of the hydrodynamic lubrication of the top compressions ring in a large two-stroke marine diesel engine has previously been performed by the authors of this article in [2]. The cyclic variation throughout one stroke for the minimum film thicknesses at different interesting locations of the piston ring surface together with the friction and the pressure distribution history were computed and presented.

This article has been made in cooperation with MAN Diesel and Turbo SE (MDT) and is presenting a new method for achieving mass conservation across the piston ring in both space and time. The long term goal of the academic study is to reveal the lubricant behavior within a large two-stroke marine diesel engine and make suggestions for a future design in lubricant injectors. Large two-stroke marine diesel engines are lubricated differently than a conventional trunk engine e.g. in automotive engines. The cylinder lubricant in large marine engines is injected at a discrete position on the liner. It is supplied at every 2nd, 3rd or maybe every 10th stroke at a discrete time and location based on the geometrical properties of the engine and the operating conditions. If the amount of lubricant is too small the piston rings will dry out leading to increased asperity contact, abrasion and increased friction as well as power loss and inadequate sealing between the combustion chamber gas and scavenging area. Furthermore scuffing of the cylinder liner could occur. If the quantity is too large the lubricant is transported into the scavenging area or end up in the combustion chamber where it is either combusted or evaporated. It is of great importance to understand the lubricant transport between the injections in order to achieve an adequate injection volume.

[1]Technical University of Denmark, Department of Mechanical Engineering, Nils Koppels Alle 404, 2800 Kgs. Lyngby, Denmark.
[2]MAN Diesel & Turbo SE, Teglholmsgade 41, 2450 Copenhagen SV, Denmark.

Corresponding author:
Hannibal Overgaard, Technical University of Denmark, Department of Mechanical Engineering, Nils Koppels Alle 404, 2800 Kgs. Lyngby, Denmark.
Email: hcover@mek.dtu.dk

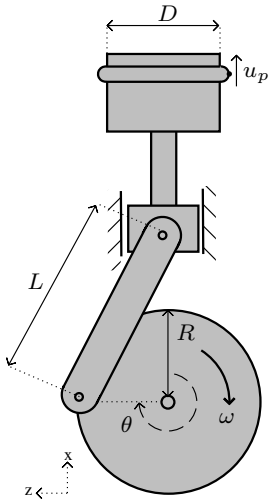

Figure 1. Crankshaft / connecting rod / crosshead / piston assembly. Engine seen from aft.

From both an economic and environmental point of view it would be reasonable to reduce the amount cylinder lubricant as it is, if combusted, an expensive fuel.

The objective of this article is to investigate the lubricant transport across the piston ring for the first three crankshaft rotations at different operating conditions. The transport will be studied for no load versus an artificial combustion load as well as a flat lubricant profile versus a lubricant injection at a discrete location. The focus will be on revealing in which strokes the lubricant transport are most significant with the distribution between the up and downstroke as well as the lubricant behavior based on the operating conditions.

Method

Basic concept

A method was proposed by [2] to model the lubricant transport along the cylinder liner in large two-stroke marine diesel engines. The method is very briefly outlined in this section. A thorough examination of the method can be found in [2].

A sketch of a piston-crankshaft assembly which could be in a large marine diesel is seen in Figure 1 with the relationship between the crankshaft rotation and the piston ring velocity

$$u_p = \omega\left(Rsin(\theta) + \frac{R^2 sin(\theta)cos(\theta)}{\sqrt{L^2 - R^2 sin^2(\theta)}}\right) \tag{1}$$

Reynolds equation

Reynolds equation is seen in Equation 2 under assumption of only the liner moving while considering the lubricant being Newtonian, isoviscous, incompressible and with constant density.

$$\frac{\partial}{\partial x}\left(h^3\frac{\partial p}{\partial x}\right) = 6u_x\eta_0\frac{\partial h}{\partial x} + 12\eta_0\frac{\partial h}{\partial t} \tag{2}$$

where h is the oil film thickness, p the oil pressure, u_x the liner velocity, η_0 the lubricant viscosity and t the time.

Film pressure distribution

Reynolds equation is solved approximately by a numerical central finite difference method of second-order with explicit time stepping where $h_{0,old}$ denotes the previous time step. The difference equation is seen in Equation 3.

$$\underbrace{\frac{h_{i+1/2}^3}{\Delta x^2}}_{A_i} p_{i+1} + \underbrace{\frac{h_{i-1/2}^3}{\Delta x^2}}_{B_i} p_{i-1} \underbrace{- \frac{h_{i+1/2}^3 + h_{i-1/2}^3}{\Delta x^2}}_{C_i} p_i = \underbrace{6u_x\eta_0\frac{h_{i+1} - h_{i-1}}{2\Delta x} + 12\eta_0\frac{h_i - h_{i,old}}{\Delta t}}_{f_i} + error(\Delta x^3) \tag{3}$$

where h is the oil film thickness, p the oil pressure, u_x the liner velocity, η_0 the lubricant viscosity, Δx the nodal distance and Δt the timestep.

The difference equation is solved as a system of linear equations as shown in Equation 4. Reynolds boundary conditions and open-end cavitation from [3] are imposed.

$$\underbrace{\begin{bmatrix} C_1 & A_1 & & & & \\ B_2 & C_2 & A_2 & & & \\ & B_3 & C_3 & A_3 & & \\ & & .. & .. & .. & \\ & & & B_{nx} & C_{nx} & A_{nx} \end{bmatrix}}_{D} \underbrace{\begin{bmatrix} p_1 \\ p_2 \\ p_3 \\ .. \\ p_{nx} \end{bmatrix}}_{p_0} = \underbrace{\begin{bmatrix} f_1 \\ f_2 \\ f_3 \\ .. \\ f_{nx} \end{bmatrix}}_{f_0} \quad \Leftrightarrow \quad p_0 = D/f_0 \tag{4}$$

where A_i, B_i, C_i and f_i are the coefficients from Equation 3 and p_0 the pressure distribution.

Force equilibrium of the piston ring

A force equilibrium of the piston ring is made. A free body diagram of the piston ring showing the forces acting in the z-direction can be seen in Figure 2. The friction force between the piston and piston ring is neglected together with all forces in the x-direction. $p_{1,gas}$ and $p_{2,gas}$ are the gas pressures, F'_{hyd} the hydrodynamic force of the oil and is computed by Equation 5, F'_{sp} is the tension spring force of the piston ring, $F'_{1,bs}$ the pressure related back-side force together with $F'_{1,fs}$ and $F'_{2,fs}$ as the pressure related piston-ring-face forces. Due to blow-by of the combustion gas across the piston ring it is assumed that $p_{2,gas} = \frac{2}{3} \cdot p_{1,gas}$.

$$F'_{hyd} = \int_{l_{hyd}} p_0 \, dx \tag{5}$$

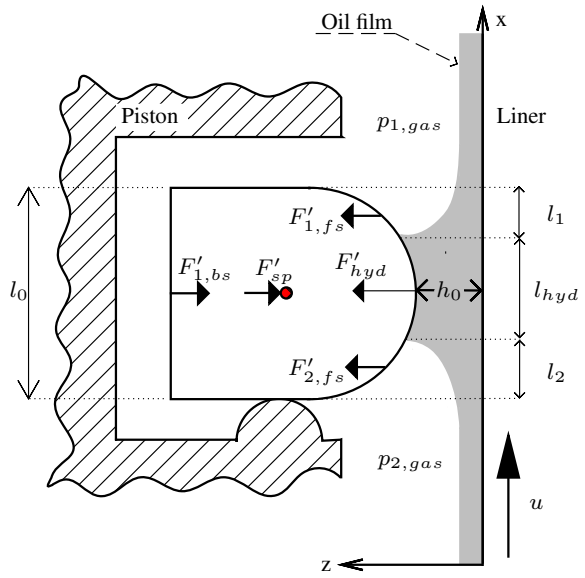

Figure 2. Free body diagram of the piston ring.

where l_{hyd} is the wetted length of the piston ring and p_0 the oil pressure distribution derived from Reynolds equation in Equation 2. The minimum film thickness, h_0, is the free parameter of the force equilibrium as it is determining F'_{hyd}.

Perturbation of Reynolds equation

The perturbation method was suggested by [4] where the assumed parabolic height profile, $h = h_0 + r(1 - cos(\phi))$, is perturbed by an infinitesimal small disturbance, Δz, so that the height profile becomes $h = (h_0 + \Delta z) + r(1 - cos(\phi))$. It should be noticed that ϕ is related to the geometry of the piston ring and not the crankshaft position. The lubricant pressure distribution is then affected by the disturbance with $p = p_0 + p_\Delta \Delta z$. The perturbed Reynolds equation can be seen in Equation 6 with respect to the perturbed pressure, p_Δ.

$$\frac{\partial}{\partial x}\left(h^3 \frac{\partial p_\Delta}{\partial x}\right) = -3\frac{\partial}{\partial x}\left(h^2 \frac{\partial p_0}{\partial x}\right) + \frac{12\eta_0}{\partial t} \tag{6}$$

where p_Δ is the perturbed pressure and p_0 the undisturbed pressure.

By integrating the perturbed pressure over the wetted length, $K_z = \int_{l_{hyd}} p_\Delta dx$, a coefficient of stiffness, K_z, can be found. The change in oil film thickness, Δz, due to the imposed disturbance is found by taking advantage of the dynamic properties of the stiffness coefficient as seen in Equation 7.

$$\begin{aligned} K_z \Delta z - \sum F'_z &= 0 \\ \Leftrightarrow \Delta z &= \frac{F'_{1,bs} + F'_{sp} - F'_{hyd} - F'_{1,fs} - F'_{2,fs}}{K_z} \end{aligned} \tag{7}$$

where K_z is the stiffness coefficient, Δz the change in oil film thickness, $\sum F'_z$ the sum of all forces in z-direction, F'_{hyd} the hydrodynamic force of the oil, F'_{sp} the tension spring force of the piston ring, $F'_{1,bs}$ the pressure related back-side force together with $F'_{1,fs}$ and $F'_{2,fs}$ as the pressure related piston-ring-face forces.

So

$$h^{new} = h + \Delta z \tag{8}$$

where h^{new} is the new film thickness, h the old film thickness and Δz the change in the film thickness.

The new minimum film thickness is inserted into the initial Reynolds equation in Equation 2 and h_0^{new} is calculated again. The iterative procedure continues until the force equilibrium is reached for a given θ. The numerical flow chart for the iterative procedure is seen in Figure 13 in Appendix.

Mass conservation

The face of the piston ring is seen in Figure 3. An initial amount of lubricant is on the liner, h_{in}^{∞}, and is assumed to be undisturbed by the piston ring and is either left behind by the piston ring in the previous stroke or injected on the liner. The undisturbed entering lubricant flow is defined as $q_{in}^{\prime\infty}$ and is calculated by the relationship between the piston ring velocity and the film thickness in Equation 9.

$$q_{in}^{\prime\infty} = u_x h_{in}^{\infty} \tag{9}$$

The lubricant that goes under the piston ring is $q'^{\star}$ and is computed as

$$q'^{\star} = \frac{u_x h^{\star}}{2} - \frac{(h^{\star})^3}{12\eta}\frac{\partial p}{\partial x} \tag{10}$$

where $h^{\star}$ is the film thickness where the wetted surface of the piston ring begins.

By an iterative procedure the starvation point e.g. the position of inlet height, $h^{\star}$, is changed to adjust the lubricant volume flow under the piston ring. In case of starvation the inlet position moves towards the center of the piston ring. When fully flooded conditions are present lubricant build up in front of the piston ring occurs. In order to account for this build up the model must be able to transfer lubricant between the different positions, θ, on the liner. A control volume is imposed as shown in Figure 3. The inlet height or starvation height for the present θ_k, $h_k^{\star}$, is represented by a dashed line. The dotted line is the starvation height at the previous position, θ_{k-1}. The oil flow at starvation height is $q'^{\star}$. The oil enters the system with the height h_{in}^{∞}. The distance between the two heights, l_{∞}, is assumed to be very large compared to the domain so that the entering flow, $q_{in}^{\prime\infty}$, is completely undisturbed by the piston ring. The two heights for the previous θ, $h_{in,k-1}^{\infty}$, $h_{k-1}^{\star}$, together with their distance, l_{∞}, forms an area or control volume marked with a dotted line in Figure 3. The area is calculated by the equation below.

$$A_{CV,\theta_{k-1}} = \frac{h_{\theta_{k-1}}^{\star} + h_{in,k-1}^{\infty}}{2} l_{\infty} \tag{11}$$

The same calculations are done for the next θ i.e. θ_k, and for maintaining mass conservation at different operation conditions a new starvation height, $h_k^{\star}$ and corresponding

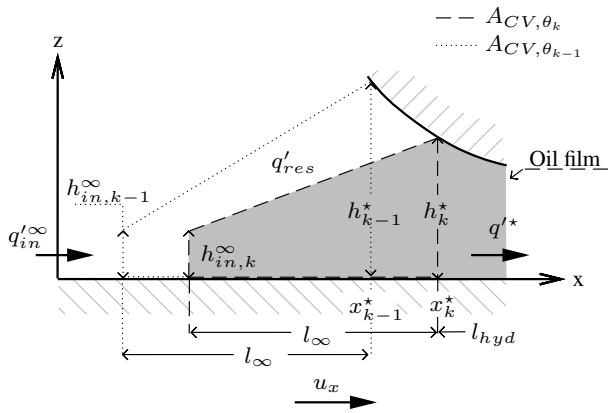

Figure 3. Lubricant control volume in front of the piston ring for transient mass conservation.

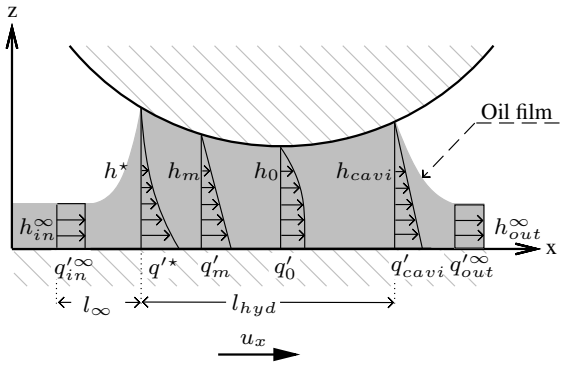

Figure 4. Flow profiles under the piston ring.

area, A_{CV,θ_k}, represented by the dashed line in Figure 3 is calculated. Between the two θ lubricant has either been build up or consumed by the piston ring. The phenomena is accounted for by the residual term, q'_{res}, which is considered as the change in area between the two θ over the timestep and is calculated by

$$q'_{res} = \frac{A_{CV,\theta_k} - A_{CV,\theta_{k-1}}}{\Delta t} = \frac{\frac{h^{\star}_{\theta_k} + h^{\infty}_{in,k}}{2} l_{\infty} - \frac{h^{\star}_{\theta_{k-1}} + h^{\infty}_{in,k-1}}{2} l_{\infty}}{\Delta t} \quad (12)$$

The transient mass conservation between the two θ is

$$\sum q' = 0 \Leftrightarrow q'^{\infty}_{in} - q'^{\star} - q'_{res} = 0 \quad (13)$$

A flow chart of the iterative procedure is seen in Figure 13 in Appendix .

All the different flow profiles can be seen in Figure 4 where q'^{∞}_{in}, $q'^{\star}$, q'_m, q'_0, q'_{cavi} and q'^{∞}_{out} corresponds to the flow at positions of the undisturbed inlet, starvation, maximum pressure with $\partial p/\partial x = 0$, minimum film thickness, cavitation and the outlet, respectively.

Triangular lubricant profile on the liner

In large two-stroke marine diesel engines the lubricating system works differently than in a conventional trunk

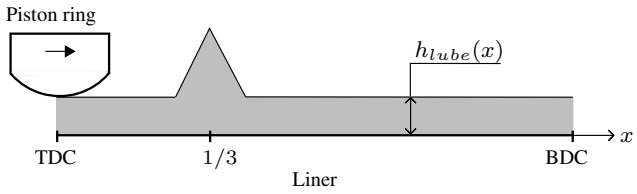

Figure 5. Sketch of a triangular lubricant injection profile on the liner for injection position $1/3$.

engine. Cylinder lubrication oil is injected from discrete located holes in the cylinder liner.

The position of the lubricant injection holes is often approximately $1/3$ from TDC. The oil film thickness on the liner is assumed to be an approximated local triangle geometry after the injection. A sketch of this is seen in Figure 5 where discrete injection position $1/3$ from TDC is sketched. The dimensions are grossly exaggerated.

For comparison between a flat and triangular lubricant profile the amount of oil injected on the liner is considered constant regardless of the geometry and position i.e.

$$V_{lube,inj} = 2\pi R \int_{BDC}^{TDC} h_{lube}(x)dx = constant \quad (14)$$

where R is the radius of the piston and h_{lube} the lubricant thickness on the liner.

Results and discussion

Operating conditions

For simulating the piston ring lubrication two different load cases have been used. The first case consider all the gas pressure related forces of the free body diagram in Figure 2 to be zero. Only the spring tension force and the hydrodynamic force of the lubricant is present. For the second case an artificial combustion pressure scenario has been implemented to imitate the real operating conditions of the piston ring regarding pressure forces. As mentioned previously it has been assumed that $p_{2,gas} = \frac{2}{3} \cdot p_{1,gas}$. The combustion pressure profile is seen in Figure 6. This study is neglecting some phenomena which are present when performing experiments i.e. the temperature dependency on the lubricant viscosity which will be commented on later together with lubricant evaporation. Furthermore the lubricant is assumed to be new, fresh and unaffected by the harsh conditions within a combustion engine during the modeling. The viscometric properties of the lubricant due to degradation has been studied by [5] which potentially affect the viscosity and thereby the load carrying capacity of the lubricant. With the assumption of a continuously supply of fresh oil the influence of particles in the lubricant does not matter. In a real system even particles much smaller than the film thickness cause wear [6] which could change the surface appearance as well as the load carrying capacity of the lubricant. Furthermore the surfaces are assumed fully

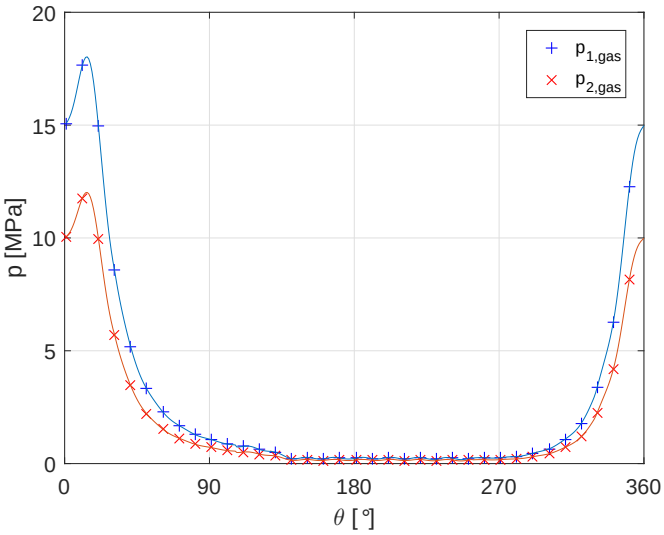

Figure 6. Combustion pressure profile above, $p_{1,gas}$, and below, $p_{2,gas}$, the piston ring.

Table 1. Values used for piston ring simulations.

Parameter	Value	Unit
D	0.8	$[m]$
η_0	50· 10^{-3}	$[Pa \cdot s]$
l_0	5	$[mm]$
L	3.72	$[m]$
N	40-100	$[RPM]$
nx	400	$[-]$
$p_{1,gas}$	0-18	$[MPa]$
$p_{2,gas}$	0-12	$[MPa]$
p_{sp}	203	$[kPa]$
r	150	$[mm]$
R	1.86	$[m]$
$V_{lube,inj}$	Constant	$[m^3]$

smooth.

Beside the two loads several lubricant injection profiles are investigated. A flat profile together with a "1/3 injection position profile" are used. For studying the influence of the loads and lubricant injection profiles a fixed radius of curvature for the piston ring of $150\ mm$ has been used. The different operating parameters are shown in Table 1.

Piston ring scraping and lubricant accumulation

Some of the different film thicknesses from Figure 4 are shown in Figure 7 as a function of the crank angle rotation for the initial down and upstroke, $0° \leq \theta \leq 360°$. The lubricant profile on the liner is illustrated with the parameter h_{in}^{∞}. The simulation has been made for flat lubricant injection both with no load in Figure 7a and combustion load in Figure 7b. Furthermore have the simulations been made for a "1/3 lubricant injection position" with no load in Figure 7c and combustion load in Figure 7d.

When looking at the film thicknesses with no load and flat profile in Figure 7a fully flooded conditions are initially present and lubricant is accumulated in front of the for $\theta \leq 20°$. It is illustrated by the line for h_{in}^{∞} being larger than the line for h_{out}^{∞}, i.e. more lubricant is entering than leaving the system indicating accumulation. From $20° \leq \theta \leq 35°$ the accumulated lubricant is consumed which leaves more oil behind than entered for the given θ. From $35° \leq \theta \leq 130°$ starved conditions are present which is seen as the inlet or starvation point, $h^{\star}$, moves towards the center of the ring. Thereby the wetted length of the piston ring is reduced in order to maintain the load carrying capacity of the lubricant.

In the first quarter of the stroke with combustion load and flat profile in Figure 7b pressure in front of the ring is up to $18\ MPa$ which results in very small film thicknesses to maintain the hydrodynamic pressure and thereby the load carrying capacity for the force equilibrium of the piston ring. A large amount of oil is accumulated which ensures that fully flooded conditions are maintained through out the entire downstroke from $0° \leq \theta \leq 180°$ where starved conditions will be present from $\theta \geq 230°$ and forth.

With no load and "1/3 injection position" in Figure 7c the result follows the one for no load and flat injection in Figure 7a. But at $\theta = 54°$ the lubricant injection peak is encountered by the piston ring which gives a lubricant build-up. The accumulated oil ensures fully flooded conditions from $54° \leq \theta \leq 80°$ after which no more build-up is present.

For the combustion load and "1/3 injection position" in Figure 7d is more or less identical with simulation of no load and flat injection in Figure 7b due to the high combustion pressures which ensure a large lubricant accumulation in either case.

The results for film thicknesses in Figure 7a and 7b are illustrated as indices in Figure 8 where the location for inlet and cavitation points on the piston ring are plotted. The gray area is the length of the active part where lubricant affects the piston ring. A location of zero or one for, respectively, the first and second stroke indicates fully flooded conditions. As mentioned previously, fully flooded conditions are maintained through half of the stroke with combustion pressure due to accumulation of lubricant with high pressures.

Residual lubricant on the liner

Simulations have been made to investigate the influence of the engine velocity on the residual lubricant left behind on the liner after three crankshaft rotations. A result of a simulation is seen in Figure 9 where the development in the lubricant on the liner has been plotted as a function of θ. The lubricant is injected at $\theta = 54°$ and the development goes from the initial lubricant injection profile on the liner to after six strokes for different engine velocities. The simulations have been made for no load and combustion load in Figure 9a and 9b respectively. The appearance of the initial profile is flat with a triangular peak around the injection position. The lubricant profile on the liner after six strokes is computed for three engine velocities i.e. $N = [40; 70; 100]\ rpm$ which corresponds to mean piston ring velocities of $u_x = [4.96; 8.68; 12.4]\ m/s$. In general for both kinds of load an increased velocity increase the 'flattening' of the

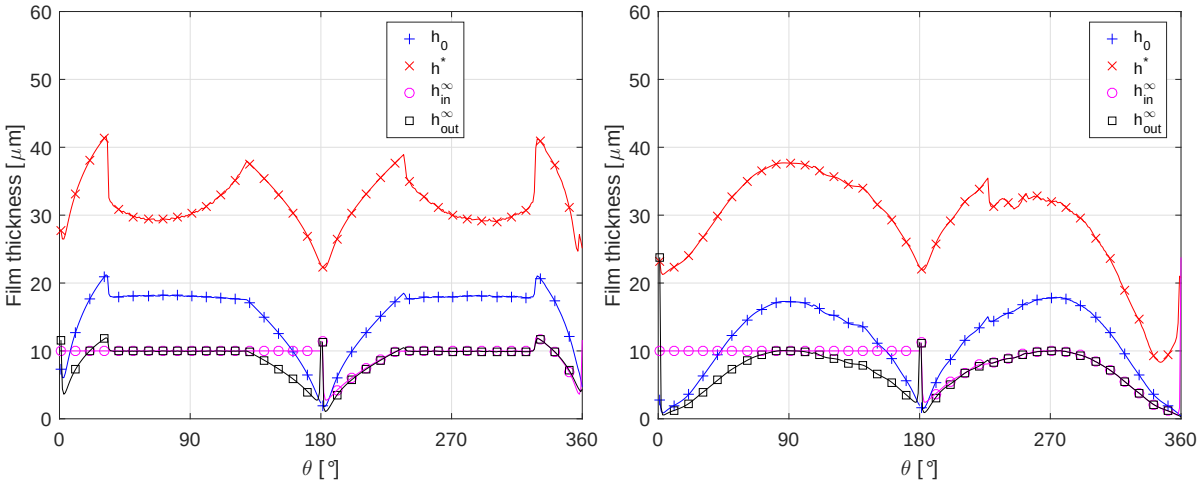

(a) Flat injection and no load.

(b) Flat injection and combustion load.

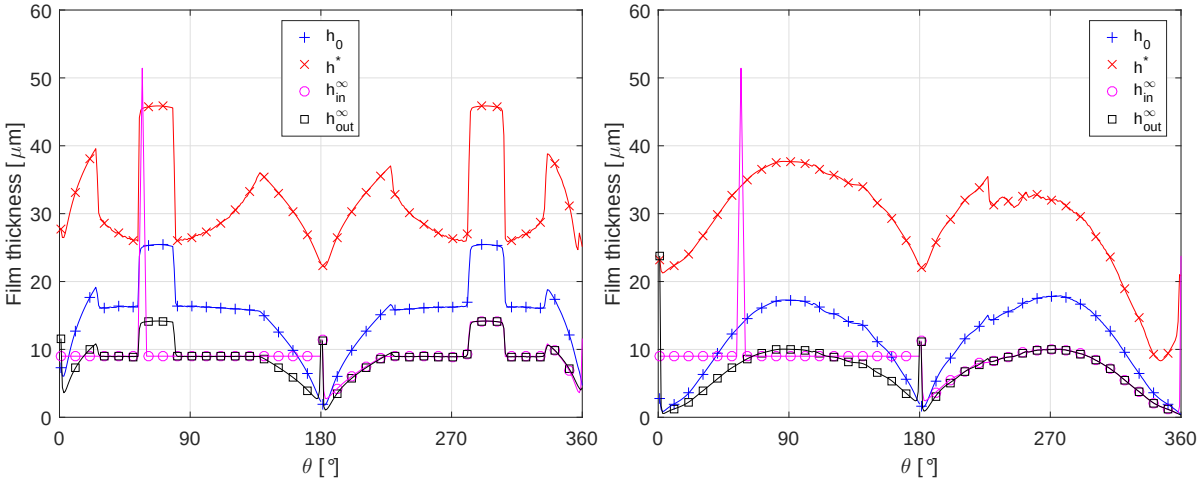

(c) 1/3 injection position and no load.

(d) 1/3 injection position and combustion load.

Figure 7. Film thicknesses at 1st crankshaft rotation as a function of θ with $N = 40\ RPM$ with both no load and combustion load as well as flat and 1/3 injection position.

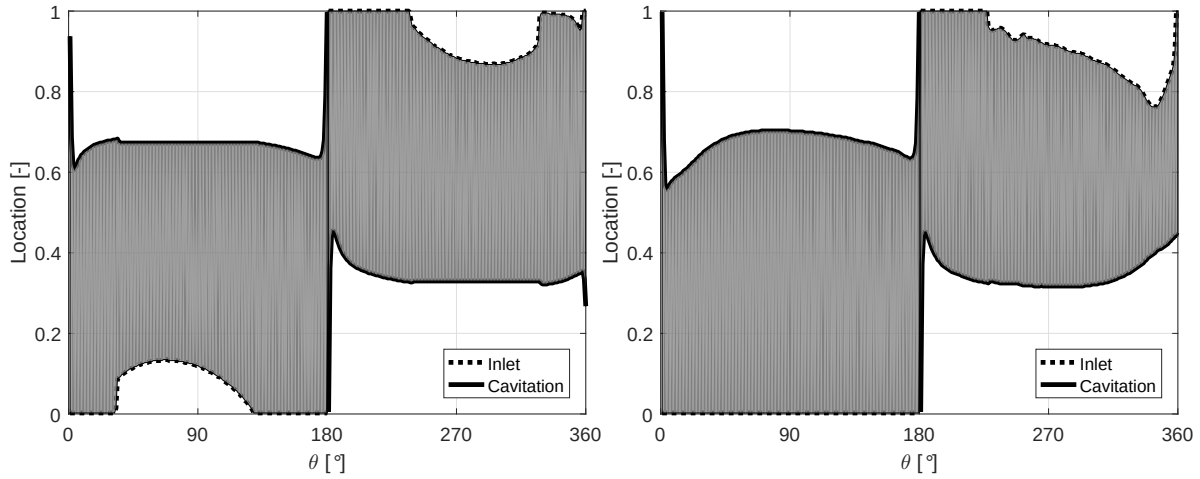

(a) No load.

(b) Combustion load.

Figure 8. Index of inlet, $h^{\star}$, and cavitation point, h_{cavi} as a function of θ for 1st crankshaft rotation with $N = 40\ RPM$ with a flat lubricant profile at different loads.

lubricant peak. However, the shape of the flattening is very dependent on the load. For no load in Figure 9a the lubricant peak deforms after six strokes but the initial position and shape is somehow preserved. The phenomenon with flattening of the injection peak is considered to be the same regardless of the position of injection. On the other hand with the combustion pressure in Figure 9b the change in the lubricant profile is significant as the lubricant is pushed

towards the center of the liner due to the high combustion pressure around TDC, the high compression pressure around BDC as well as the low velocity around both TDC and BDC. The lubricant has some small peaks for $N = [40; 70]\ RPM$ at around $\theta = 130°$ where a pressure drop occurs in Figure 6.

Lubricant consumption

Lubricant consumption is present where the scraped oil is not utilized before end of the stroke. The consumption is defined as the change in the lubricant amount on the liner from the initial injection to after three crankshaft rotations. The behavior of the consumption as a function of the engine speed and injection profile has been investigated.

The lubricant consumption is illustrated in Figure 10 for both kinds of load and both lubricant injection profiles. The consumption is illustrated for each stroke up to three crankshaft rotations. The tendency for flat injection in Figure 10a and "1/3 injection position" in Figure 10b are more or less similar to each other. The major part of the consumption takes place in the initial downstroke and the minor part in the following upstroke of the first crankshaft rotation after which steady-state occurs. From the second rotation and forth the lubricant consumption will be steady until additional lubricant is injected.

Figure 11 shows the total lubricant consumption after three crankshaft rotations at different engine speeds for flat and "1/3 injection position". For no load and flat injection in Figure 11a the consumption decreases from $10 \rightarrow 5\ \%$ when the speed is increased from $40 \rightarrow 100\ RPM$. When simulating with combustion pressure the tendency is similar as the lubricant consumption is decreased from $36 \rightarrow 16\ \%$ when the speed is increased from $40 \rightarrow 100\ RPM$. When changing the lubricant injection from flat profile to "1/3 injection position" profile in Figure 11b the behavior of the consumption is more or less the same where the consumption has increased af few percent for combustion load and decreases a bit with no load. In general the lubricant consumption is larger when running with combustion load compared to no load. This tendency is strongly influenced by the high pressures of the combustion load which, as mentioned previously, results in low film thicknesses to maintain the force equilibrium of the piston and a large amount of lubricant is accumulated in front of the ring.

The results for lubricant consumption in Figure 12 is expanded to illustrate the overall distribution between down- and upstroke. For the no load and flat profile situation in Figure 12a the primary stroke for lubricant consumption is the downstroke for all engine velocities but the distribution will even out a bit with increased velocities.

For the other scenarios i.e. combustion load and flat injection, no load and "1/3 injection position" as well as combustion load and "1/3 injection position" in, respectively, Figure 12b, 12c and 12d, the tendencies are similar to the scenario discussed before where the downstroke holds the majority of the consumption and evens out a bit with increased velocity.

The reason for the downstroke to have the major lubricant consumption is highly influenced by one particular assumption of the numerical model. For doing these simulations a downstroke is considered to be the initial stroke. If the running conditions results in low film thicknesses at the initial downstroke a large amount of lubricant is accumulated in front of the ring which might not be utilized before end of the stroke and is therefore lost. If the engine velocity is increased a larger lubricant pressure will be build-up beneath the piston ring. To overcome this pressure increase the film thickness increases which allows more lubricant to pass under the ring and not being scraped off. The amount of passed lubricant will then be scraped off in the following upstroke and therefore the distribution becomes more even with increased velocities.

Lubricant film thicknesses

The minimum film thicknesses computed and presented in Figure 7 have averages of $h_{0,mean} \approx 15\ \mu m$ which might seem rather high compared to some studies e.g. [7] and [8] where the average oil film thicknesses were some few microns. The most significant difference with respect to the operating conditions from the previous mentioned studies and this article is that the influence of the temperature on the viscosity. Not surprisingly the viscosity as a function of the temperature is important due to its significant role in the pressure generation from Reynolds equation in Equation 2.

On the other hand, studies where the viscosity has been considered independent of the temperature e.g. [1] calculate minimum film thicknesses in the same order of magnitude as this article.

Conclusion

The following conclusion have been drawn:

(i) A transient mass conservation for lubrication of the piston ring was imposed in the numerical model. It has shown able to account for lubricant scraped and accumulated in front of the ring together with the following lubricant consumption.
(ii) The kind of load e.g. no load versus combustion load has shown to have significant influence on the appearance of the residual lubricant film on the liner.
(iii) The downstroke has shown to be the major lubricant consumer with the following upstroke as the minor one. Steady-state conditions regarding the lubricant consumption appears after the first crankshaft rotation and forth.

Funding

This project has received funding from the European Unions Horizon 2020 research and innovation program under grant agreement No 634135.

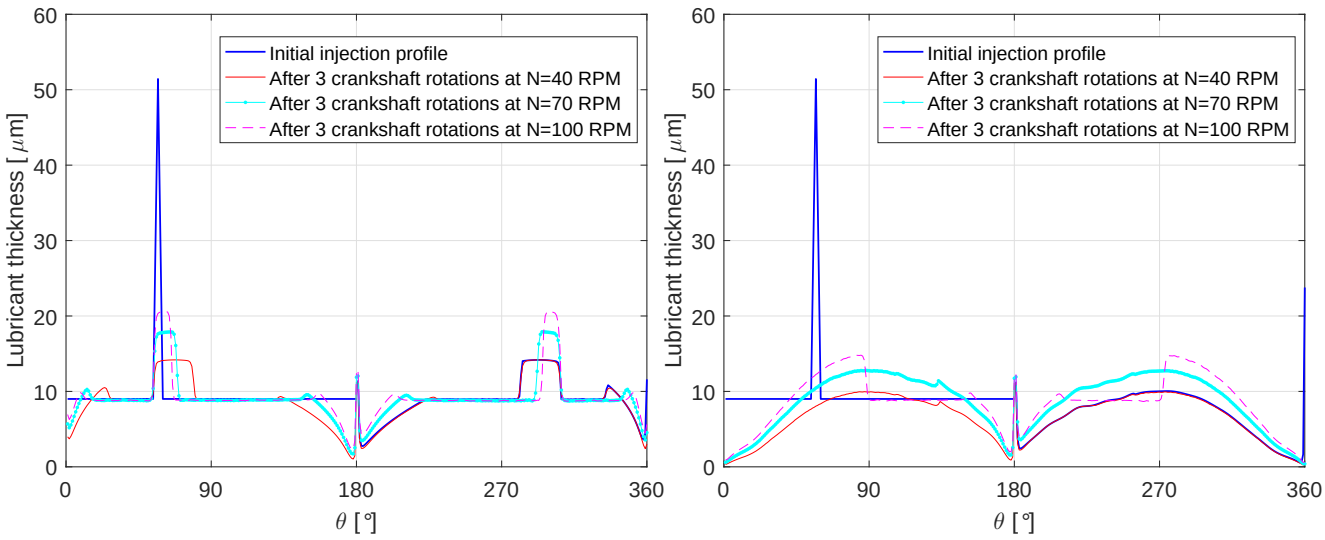

(a) No load. **(b)** Combustion load.

Figure 9. Development in the lubricant profile on the liner as a function of θ after three crankshaft rotations with 1/3 injection position for both no load and combustion load.

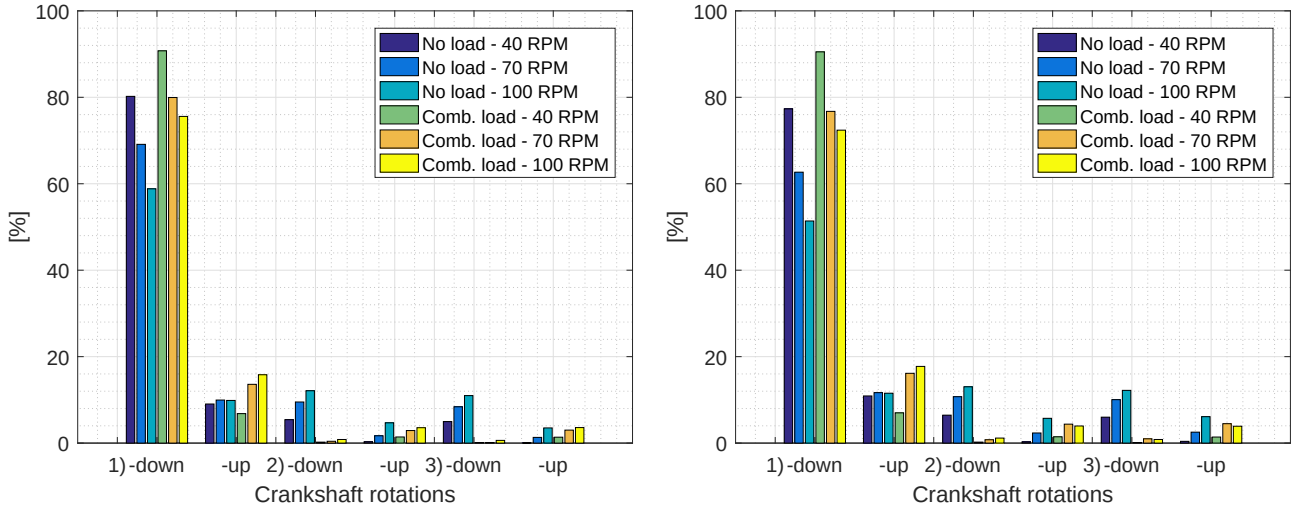

(a) Flat injection. **(b)** 1/3 injection position.

Figure 10. Relative lubricant consumption in [%] for each stroke up to six strokes for flat and 1/3 injection position, both no load and combustion load and different engine speeds. The lubricant consumption is relative to the total amount consumed after three crankshaft rotations.

Declaration of conflicting interests

The Authors declare that there is no conflict of interest.

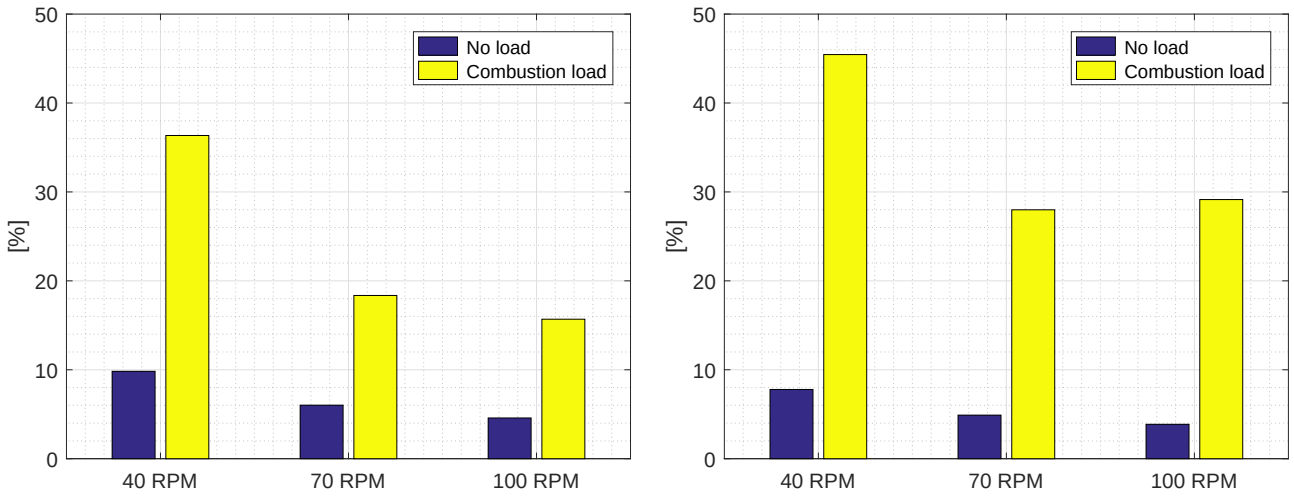

(a) Flat injection.

(b) 1/3 injection position.

Figure 11. Total lubricant consumption in $[\%]$ after tree crankshaft rotations, flat and 1/3 injection position, both no load and combustion load and different engine speeds.

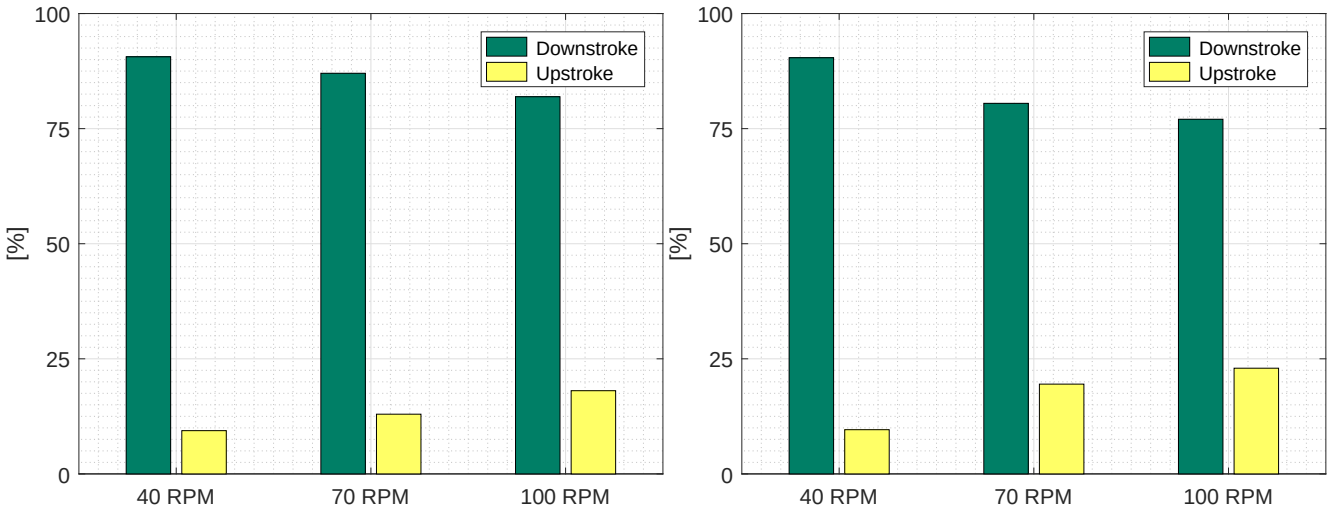

(a) No load and flat injection.

(b) Combustion load and flat injection.

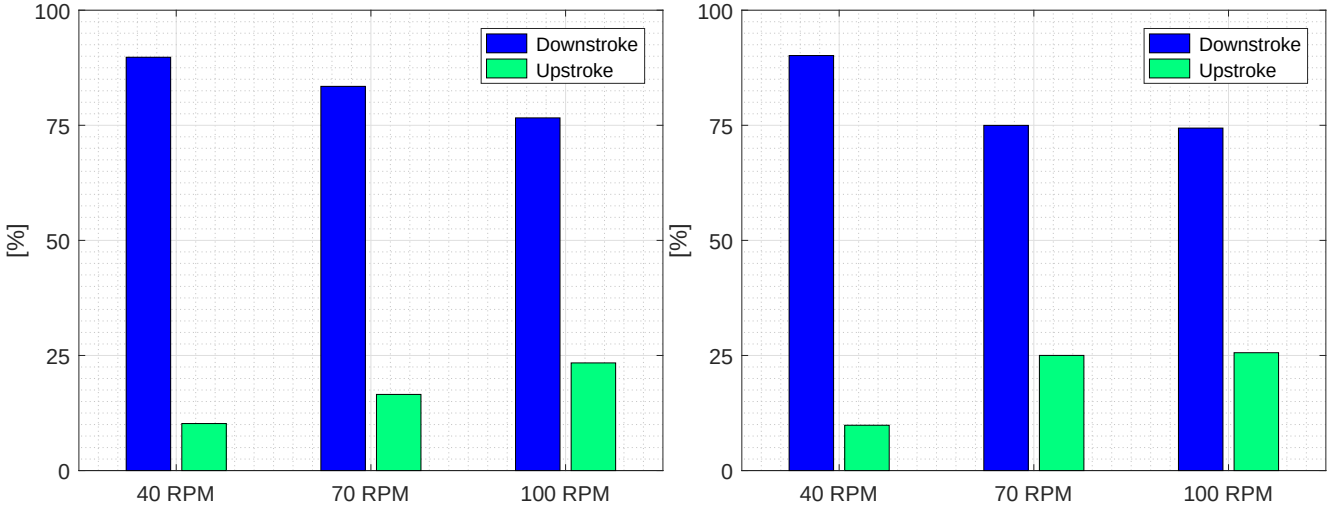

(c) No load and 1/3 injection position.

(d) Combustion load and 1/3 injection position.

Figure 12. Relative lubricant consumption distribution in $[\%]$ between down and upstroke after three crankshaft rotations, flat and 1/3 injection position, both no load and combustion load and different engine speeds.

References

1. Hamrock B J and Esfahanian M (1998), On the Hydrodynamic Lubrication Analysis of Piston Rings, *Lubrication Science 10-4*, August, p. 265–286.

2. Overgaard H, Klit P and Vølund (2016), Investigation of Different Piston Ring Curvatures on Lubricant Transport along Cylinder Liner in Large Two-Stroke Marine Diesel Engines, *submitted to Proceedings of the Institution of Mechanical Engineers, Part J: Journal of Engineering Tribology*, NordTrib 2016 - Proceedings of The 17th Nordic Symposium on Tribology.
3. Han D C and Lee J S (1998), Analysis of the piston ring lubrication with a new boundary condition, *Tribology International*, 12, p. 753–760, 31.
4. Lund J W and Thomsen K K (1978), A Calculation Method and Data for the Dynamic Coefficients of Oil-Lubricated Journal Bearings, *The Design Engineering Conference*, Topics in Fluid Film Bearing and Rotor Bearing System Design and Optimization, p. 1–12.
5. Taylor R I and Bell J C (1994), The Influence of Lubricant Degradation on Friction in the Piston Ring Pack, *Tribology Series*, C, p. 531–536, 27.
6. Jacobson B O (1991), Lubricant contamination, *Rheology and Elastohydrodynamic Lubrication*, p. 341–351, Elsevier Science Ltd, ISBN 978-0444881465.
7. Froelund K, Schramm J, Tian T, Wong V and Hochgreb S (2001), Analysis of the Piston Ring / Liner Oil Film Development During Warm-Up for an SI-Engine, *Journal of Engineering for Gas Turbines and Power*, January 2001, p. 109–116, 123.
8. Froelund K, Schramm J, Noordzij B, Tian T and Wong V (1997), An Investigation of the Cylinder Wall Oil Film Development During Warm-Up of an SI-Engine Using Laser Induced Fluorescence, *Understanding Engine Oil Rheology and Tribology, SAE International*, May 1997, p. 75–83, 971699.

Appendix

The nomenclature is seen in Table 2.

The flow chart of the numerical algorithm with transient mass conservation is seen in Figure 13.

Table 2. Nomenclature.

Parameters	
BDC	Bottom dead center, $[-]$
D	Piston diameter, $[m]$
F′	Force per unit circumference, $[\frac{N}{m}]$
h	Oil film thickness, $[m]$
K	Stiffness coefficient, $[\frac{N}{m^2}]$
l	Length of piston ring, $[m]$
L	Connecting rod length, $[m]$
N	Crankshaft rotational speed, $[RPM]$
nx	Number of discretization points, $[-]$
p	Pressure, $[Pa]$
$p_{1,gas}$	Gas pressure, above piston ring, $[Pa]$
$p_{2,gas}$	Gas pressure, below piston ring $[Pa]$
q′	Volume flow per unit circumference, $[\frac{m^2}{s}]$
r	Piston ring radius of curvature $[m]$
R	Crankshaft radius, $[m]$
s_h	Shoulder height, $[m]$
t	Time, $[s]$
TDC	Top dead center, $[-]$
u_x	Liner velocity, $[\frac{m}{s}]$
u_p	Piston velocity, $[\frac{m}{s}]$
Subscripts	
0	Initial/index
bs	Back-side
cav	Cavitation
fs	Piston ring face side
hyd	Hydrodynamic
i	Index, spatial
in	Inlet from previous θ or stroke
k	Index, time
m	At $max(pressure)$ and $\partial p/\partial x = 0$
min	Minimum
out	Outlet for next θ or stroke
res	Residual
sp	Elastic spring tension
x	x-direction
z	z-direction
Superscripts	
∞	Outlet / inlet
$'$	Per unit circumference
$\star$	Starvation point
Greek letters	
Δ	Difference
η_0	Absolute viscosity, $[Pa \cdot s]$
ω	Crankshaft angular velocity, $[s^{-1}]$
ϕ	Piston ring geometry parameter, $[^\circ]$
θ	Crank angle degree (CAD), $[^\circ]$

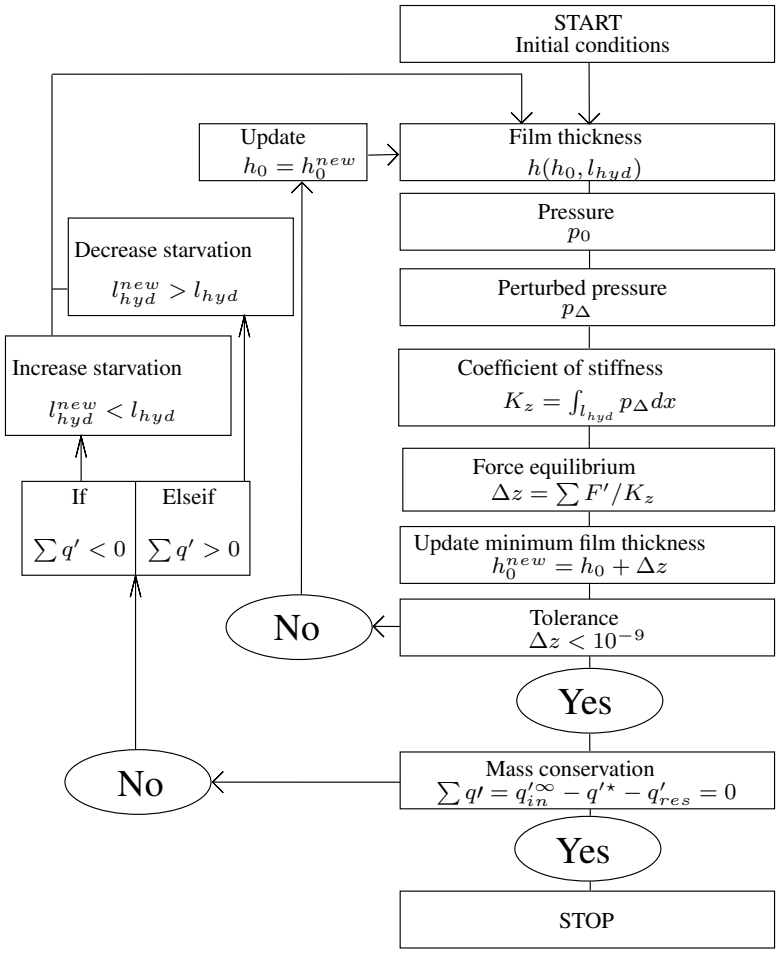

Figure 13. Flow chart of the numerical algorithm with transient mass conservation.